Self-Assembly

DOI: 10.1002/anie.200703628

Siliceous Nanopods from a Compromised Dual-Templating Approach**

*Sui Yang, Xufeng Zhou, Pei Yuan, Meihua Yu, Songhai Xie, Jin Zou, Gao Qing Lu, and Chengzhong Yu**

In nature, crystalline mineral solids are ordered in microstructures and usually have highly regular shapes which reflect the well-defined arrangements of atoms or molecules. On the other hand, materials produced by living creatures, or the micro-organisms themselves, generally exhibit complex morphologies and possess advanced biofunctionalities. Using the self-assembly and supramolecular templating approach to fabricate artificial materials that mimic biological systems is an intensely investigated topic in material science.[1,2] For example, liquid-crystal templating methods[3,4] lead to ordered mesoporous materials with crystal-like shapes[5] and helical structures,[6] while vesicle templating as well as colloidal templating give rise to hollow spheres[7,8] or ordered macroporous materials.[9] Nevertheless, despite the successes with current synthesis strategies to obtain ordered structures, it is still difficult to fabricate complex materials that mimic biological systems by only one templating method.

Herein, we report the synthesis of a siliceous structure with an unusual silkworm cocoon-like morphology (called nanopods hereafter). Such a complex hollow structure with multiple shells and well-oriented nanochannels has been carefully characterized. Moreover, a general compromised dual-templating mechanism is proposed to direct the formation of complex structures.

Siliceous nanopods were synthesized by using cetyltrimethylammonium bromide (CTAB) and perfluorooctanoic acid (PFOA) as cotemplates in a PFOA/CTAB weight ratio (R) of 0.2. A scanning electron microscopy (SEM) image of calcined nanopods shows a high yield of oblate particles (Figure 1a). The higher-magnification SEM image (Figure 1b) shows clearly the ellipsoidal morphology, similar to that of silkworm cocoons (Figure 1a, inset), although the scale is different between the two materials. Several partially broken particles can also be seen, as indicated by the white arrows in Figure 1b, suggesting that the nanopods have hollow cores inside with relatively robust shells. The length of the nanopods is in the range of about 100–300 nm, and the width ranges from about 50 to 150 nm.

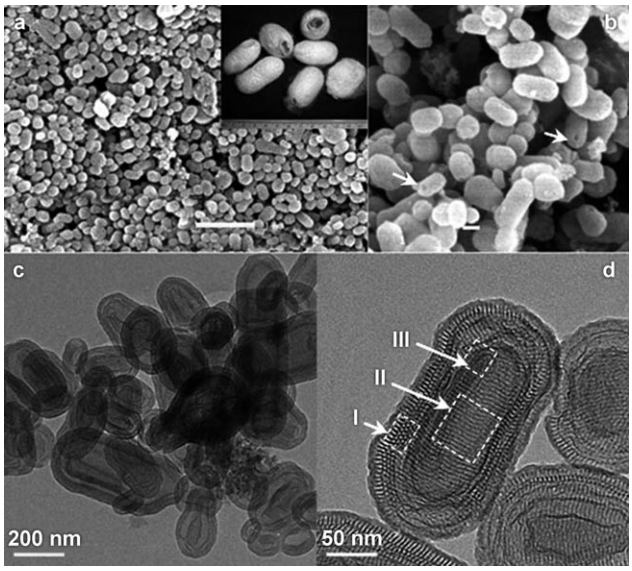

Figure 1. SEM images (a,b) and TEM images (c,d) of calcined nanopods. Scale bar is 1 μm in (a) and 100 nm in (b). The inset of (a) is a digital camera image of silkworm cocoons. The white arrows in (b) show partially broken particles (see the main text).

Transmission electron microscopy (TEM) was employed to observe the detailed microstructure of the nanopods. Figure 1c is a low-magnification TEM image and shows that the nanopods possess complex core–shell structures. Within each ellipsoidal structure, the hollow cavity is surrounded by multistructured walls. The detailed wall structure can be observed in higher-magnification TEM images (for example, Figure 1d). When the two tip regions of the ellipsoid are not considered, the structural features of the nanopod body are reflected mainly by three regions (indicated by arrows and rectangle frames). Region I at the edge shows a nearly hexagonally arrayed mesostructure viewed along the [001] direction. The stripelike image as represented in region II in the middle of the ellipsoid is also in accordance with the hexagonal mesostructure viewed along the [110] direction, and the channels are parallel to the short axis of the ellipsoid. The d spacing is estimated to be 3.9 nm, in accordance with

[*] S. Yang,[+] X. F. Zhou,[+] P. Yuan, M. Yu, S. Xie, Prof. C. Z. Yu
Department of Chemistry and Shanghai Key Laboratory of Molecular Catalysis and Innovative Materials
Fudan University, Shanghai 200433 (China)
Fax: (+86) 21-6564-1740
E-mail: czyu@fudan.edu.cn
Dr. J. Zou
School of Engineering and Centre for Microscopy and Microanalysis, the University of Queensland
QLD 4072 (Australia)
Prof. G. Q. Lu
ARC Centre of Excellence for Functional Nanomaterials, the University of Queensland, QLD 4072 (Australia)
[+] These authors contributed equally to this work.

[**] This work is supported by the State Key Research Program (2004CB217800, 2006CB932302), the NSF of China (20573021, 20421303), the Shanghai Science Committee, NCET, and FANEDD.
Supporting information for this article is available on the WWW under http://www.angewandte.org or from the author.

the X-ray diffraction (XRD) results (Figure S1 in the Supporting Information). Moreover, in region III, which is adjacent to the outer shell, an inner shell with a multilamellar structure is also clearly seen. The inner-shell structure is much clearer in the lower-magnification TEM image and can be seen in Figure 1c for nanopods with different sizes.

For nanopods with complex structures, it is difficult to determine the structural information directly by conventional TEM and XRD measurements. We therefore employed the electron tomography technology to visualize the nanopods in three dimensions.[10] A movie of one nanopod (as movie file in the Supporting Information) illustrates the entire TEM tilt series ranging from -60 to $+60°$ at an interval of 1°. Figure 2a–g shows TEM images of the nanopod recorded at different tilt angles. The tilt axis is kept parallel to the long axis of the ellipsoidal particle during the entire tilt series.

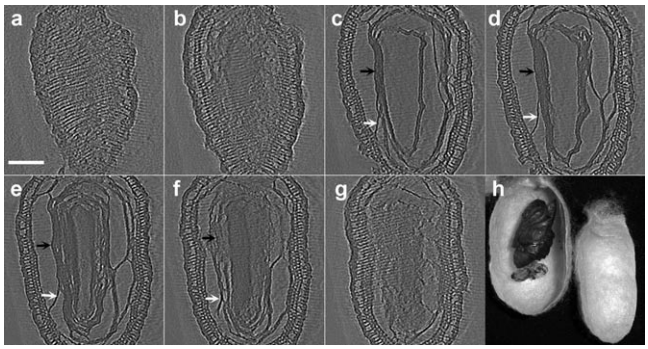

Figure 2. TEM images of a nanopod taken at different tilt angles with the same magnification: a) -60; b) -45; c) -15; d) 0; e) 15; f) 30; g) 45°. Scale bar in (a) is 50 nm. Digital camera image (h) of a silkworm cocoon cut into two halves. See the main text for discussion of the black and white arrows in (c)–(f).

Figure 2a shows that the nanochannels wrap along the short axis of the ellipsoid (taken at $-60°$). By comparing the images in Figure 2a–d (tile angles: -60 to 0°), it can be seen that the width of the ellipsoidal particle is increased, indicating that the nanopod has indeed an oblate ellipsoidal morphology. Figure 2a is probably viewed along the "long" short axis, and the sample height is thick; thus, the nanochannels are distinctly clear. With gradual tilting along the long axis of the ellipsoid, the sample height gradually decreases. As a consequence, the shell architectures appear in different patterns. Figure 2b shows both the hexagonal dotlike and stripelike arrays, while the multishell structure is clearly seen in Figure 2c–e ($\pm 15°$). The hexagonally arrayed wall thickness is about 20 nm, consisting of four to five layers of rodlike micelles. The images shown in Figure 2c–e are probably viewed along the "flat" short axis of the ellipsoid; thus, the shell structures are clearly observed. Further increasing the tilt angle again shows both the dotlike and stripelike arrays as shown in Figure 2g ($+45°$).

In addition to the outer shell with a hexagonal array, an inner shell with a multilamellar vesicular structure is also observed in the tilt series. From Figure 2c to Figure 2f with a total tilt angle of 45°, the inner linelike structure marked by black arrows (more evidently in Figure 2c) gradually turns out to be a facelike multilamellar structure (more evidently in Figure 2f). From the tilt series, it is also evident that the inner multilamellar vesicular structure is not spherical, but with a long tubular structure. The connection between the inner- and outer-shell architecture is also observed in Figure 2c–f (shown by white arrows).

The electron tomography results clearly show that the nanopods are oblate ellipsoidal hollow structures with inner multilamellar core and outer hexagonal wall architectures, thus resembling that of silkworm cocoons (Figure 2h) in which the pupae are enwrapped by tightly wound silk fibers that form closed ellipsoids. Moreover, the outer hexagonal structures are well-aligned, wrapping along the short axis of the ellipsoid in the body; thus, the hexagonal dotlike (region I) and stripelike pattern (region II) can be observed at the edge and in the middle part, respectively.

The tip region of the nanopod shows different features compared to the body. Either disordered pore structures or, in some cases, multilamellar structures are observed at the tip region (see Figure S2 in the Supporting Information). This multilamellar structure of the outer shell at the tip region should be distinguished from the multilamellar vesicular structure of the inner-wall architectures (region III in Figure 1). It is impossible to form a spherical surface from aligned hexagonal structures; thus, a disordered hexagonal or multilamellar topology is spatially favored at the tip region.

To understand the formation mechanism of nanopods, the samples synthesized at different R values are considered. Previously, we demonstrated that helical hexagonal mesostructured silicas can be obtained when $R \leq 0.1$.[11] We further synthesized samples at $R > 0.2$. When $R = 0.25$, TEM studies reveal that multilamellar vesicles with both spherical and tubular shapes are obtained (Figure 3a). The diameters of the

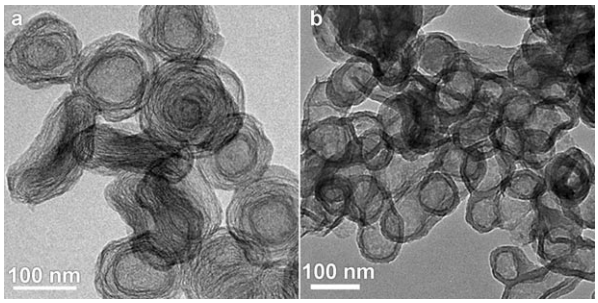

Figure 3. TEM images of calcined samples synthesized at different R values. a) $R = 0.25$ b) $R = 0.5$.

hollow concentric silica spheres are about 70–100 nm, and the distance between multilayered silica walls is estimated to be 4–6 nm, similar to the structure of reported hollow concentric vesicles.[12] When R is increased to 0.5, hollow silica spheres with single walls can be obtained as confirmed by the TEM image (Figure 3b). The particle sizes of unilamellar vesicles are smaller than that of multilamellar vesicles, as shown in Figure 3a. This vesicular structure evolution is similar to the transformation of vesicles in block copolymer studies.[13] The siliceous structures synthesized at different R values are further confirmed by the XRD patterns (Figure S1 in the

Supporting Information) and the nitrogen sorption isotherms (Figure S3 in the Supporting Information). Their physicochemical parameters are shown in Table S1 in the Supporting Information for comparison.

From these results, it is concluded that, with increasing R value (from 0.05 to 0.5), the self-assembled materials obtained from PFOA and CTAB cotemplates undergo a transformation from the helical hexagonal mesostructure to the vesicular structures. The formation of nanopods ($R = 0.2$) is a transition point of this structural evolution. In a previous study, Israelachvili and co-workers[14] proposed a geometric packing model, in which the organization of surfactant molecules is described by the packing parameter (g): $g = V/al$, where V is the effective volume of the surfactant tail region, a refers to the effective head-group area at the micelle surface, and l is the surfactant tail length. The value of g may determine the structure of self-assembled surfactant aggregates as well as surfactant-templated composite materials. The structural transformation as a function of R observed in our experiments may be explained by the g concept as illustrated in Scheme 1.

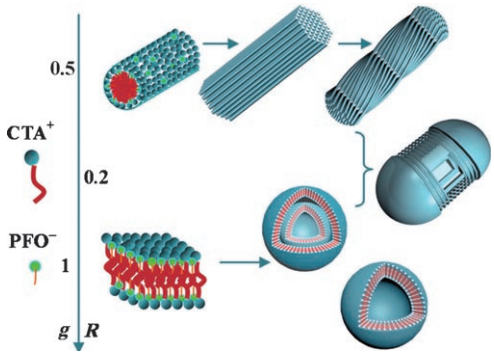

Scheme 1. Schematic illustration of the formation of nanopods through a compromised dual-templating approach.

The aggregation behaviors between CTAB and PFOA have been carefully investigated.[15] Under basic conditions during our synthesis, the cationic surfactant CTA^+ has a strong electrostatic interaction with PFO^-, which can be elucidated by FTIR studies (Figure S4 in the Supporting Information). The carbonyl stretching band of pure PFO^- appears at about 1692 cm^{-1}. This peak cannot be observed in as-synthesized MCM-41 samples obtained in the absence of PFOA. In contrast, the as-synthesized materials obtained at different R values exhibit the band at a lower frequency (1682 cm^{-1}). This red-shift of the resonances for the carbonyl group may be considered as evidence for the interaction between PFO^- and CTA^+ in our synthetic system.[16,17] Additionally, the relative intensity of this signal increases with increasing R value, in accordance with the increasing percentage of PFO^- molecules interacting with CTA^+.

The interaction between PFO^- and CTA^+ may counteract part of the cationic charges in the CTA^+ molecules, and thus a is decreased. In addition, the PFO^- molecules may insert into the hydrophobic part of the mixed micelles (increasing V). However, when $R \leq 0.1$, the small amount of PFO^- may be insignificant to change the hexagonal packing of cylindrical micelles ($g = 0.5$). The PFO^- molecules mainly play a role in reducing the surface free energy and promoting the formation of helical morphology, as we proposed previously.[11] When the R value is adjusted to 0.25–0.5, the g value is increased and the bilayer structure ($g = 1$) is favored. Eventually, the reduction of the line tension leads to the closure of bilayers and the formation of vesicular structures.[18,19]

The above discussion provides an explanation for the structure transformation from the hexagonal to the vesicular structures. However, it does not account for the formation of nanopods with the unusual morphology. As can be seen from Scheme 1, a synthetic condition for the formation of nanopods ($R = 0.2$) is a midpoint between the formation of a hexagonal mesostructure and a multilamellar vesicular structure. A simple interpretation is that, during the synthesis at $R = 0.2$, the multilamellar vesicular structure coexists with the hexagonal mesostructure. Nevertheless, the specific inner multilamellar and outer hexagonal multiwall architectures of nanopods should be addressed in more detail.

A key starting point to understand the multiwall structure feature of nanopods is the phase behavior of surfactants and their templated organic–inorganic composite structures. In our synthesis, the starting concentration of the surfactants is rather low (ca. 6×10^{-3} mol L^{-1}). While the vesicular structure is obtained by vesicular templating (VT),[7] the hexagonal mesostructure should be assembled by the cooperative liquid-crystal templating (LCT) between siliceous species and surfactants.[3,20] It is important to note that the vesicular structures are formed in dilute solutions while the liquid-crystal phases are formed in concentrated solutions,[18] two distinctly different regions in the phase diagram of surfactants. We propose that the formation of nanopod structures is through the delicate interplay of both the hexagonal and multilamellar structures (governed by the g value). The multilamellar structure formed in dilute solutions may serve as the "nucleation" site for the further deposition of a hexagonal liquid-crystal mesostructure (governed by the phase behavior), thus giving rise to nanopods with complex wall structures (Scheme 1).

To fabricate materials with complex morphologies, we further propose that the combination of two or more self-assembly methods (such as the VT and LCT dual-templating approach in our case) is more acceptable and effective compared to a single templating method. In the process of VT and LCT dual templating, it is crucial to consider a synthesis system in which the LCT and VT may compete (e.g. by changing the R value in our synthesis). Materials with complex structures and morphology (e.g. nanopods) are anticipated at a balanced midpoint where different structure organizations are compromised (e.g. at $R = 0.2$).

Importantly, there are different liquid-crystal structures, such as close-packed cubic structures of spherical micelles ($g = 1/3$) as well as the hexagonal structures.[21] The vesicular structures are also rich in uni- and multilamellar vesicles with different shapes.[12,22] We believe that our proposed dual-templating approach can be generally applied to other systems. By choosing other templating agents and a combination of different liquid-crystal and vesicular structures,

more unprecedented materials with novel structure and morphology can be designed and fabricated.

Experimental Section

Siliceous nanopods were synthesized under basic conditions by using PFOA and CTAB as cotemplates with different PFOA/CTAB weight ratios *R*. In a typical synthesis, CTAB (0.20 g) was dissolved in deionized water (96 g) with stirring at room temperature. Aqueous NaOH solution (0.70 mL, 2 M) and PFOA (0.04 g) were then added separately to the solution ($R = 0.2$). The temperature of the solution was raised and kept at 80 °C. To this solution, tetraethyl orthosilicate (1.34 mL) was added. The mixture was continuously stirred for an additional 2 h. The resulting products were collected by filtration and dried at room temperature. The templates were removed by calcination at 550° for 5 h. To understand the formation mechanism, more materials were synthesized at different *R* values by changing the amount of PFOA while the other reaction conditions remained the same.

Received: August 9, 2007
Published online: October 10, 2007

Keywords: mesoporous materials · nanostructures · self-assembly · silica · transmission electron microscopy

[1] S. Mann, G. A. Ozin, *Nature* **1996**, *382*, 313 – 318.
[2] E. Dujardin, S. Mann, *Adv. Mater.* **2002**, *14*, 775 – 788.
[3] C. T. Kresge, M. E. Leonowicz, W. J. Roth, J. C. Vartuli, J. S. Beck, *Nature* **1992**, *359*, 710 – 712.
[4] J. Y. Ying, C. P. Mehnert, M. S. Wong, *Angew. Chem.* **1999**, *111*, 58 – 82; *Angew. Chem. Int. Ed.* **1999**, *38*, 56 – 77.
[5] C. Z. Yu, B. Z. Tian, J. Fan, G. D. Stucky, D. Y. Zhao, *J. Am. Chem. Soc.* **2002**, *124*, 4556 – 4557.
[6] S. Che, Z. Liu, T. Ohsuna, K. Sakamoto, O. Terasaki, T. Tatsumi, *Nature* **2004**, *429*, 281 – 284.
[7] D. H. W. Hubert, M. Jung, P. M. Frederik, P. H. H. Bomans, J. Meuldijk, A. L. German, *Adv. Mater.* **2000**, *12*, 1286 – 1290.
[8] H. P. Hentze, S. R. Raghavan, C. A. McKelvey, E. W. Kaler, *Langmuir* **2003**, *19*, 1069 – 1074.
[9] B. T. Holland, C. F. Blanford, A. Stein, *Science* **1998**, *281*, 538 – 540.
[10] J. R. Kremer, D. N. Mastronarde, J. R. McIntosh, *J. Struct. Biol.* **1996**, *116*, 71 – 76.
[11] S. Yang, L. Z. Zhao, C. Z. Yu, X. F. Zhou, J. W. Tang, P. Yuan, D. Chen, D. Y. Zhao, *J. Am. Chem. Soc.* **2006**, *128*, 10460 – 10466.
[12] H. W. Shen, A. Eisenberg, *Angew. Chem.* **2000**, *112*, 3448 – 3450; *Angew. Chem. Int. Ed.* **2000**, *39*, 3310 – 3312.
[13] L. Chen, H. W. Shen, A. Eisenberg, *J. Phys. Chem. B* **1999**, *103*, 9488 – 9497.
[14] J. N. Israelachvili, D. J. Mitchell, B. W. Niham, *J. Chem. Soc. Faraday Trans. 2* **1976**, *72*, 1525 – 1568.
[15] H. T. Jung, S. Y. Lee, E. W. Kaler, B. Coldren, J. A. Zasadzinski, *Proc. Natl. Acad. Sci. USA* **2002**, *99*, 15318 – 15322.
[16] A. F. Thunemann, *Langmuir* **2000**, *16*, 824 – 828.
[17] B. Y. Ren, Z. Tong, X. X. Liu, C. Y. Wang, F. Zeng, *Langmuir* **2004**, *20*, 10737 – 10743.
[18] M. Antonietti, S. Forster, *Adv. Mater.* **2003**, *15*, 1323 – 1333.
[19] U. Seifert, K. Berndl, R. Lipowsky, *Phys. Rev. A* **1991**, *44*, 1182 – 1202.
[20] A. Monnier, F. Schuth, Q. Huo, D. Kumar, D. Margolese, R. S. Maxwell, G. D. Stucky, M. Krishnamurty, P. Petroff, A. Firouzi, M. Janicke, B. F. Chmelka, *Science* **1993**, *261*, 1299 – 1303.
[21] J. W. Tang, X. F. Zhou, D. Y. Zhao, G. Q. Lu, J. Zou, C. Z. Yu, *J. Am. Chem. Soc.* **2007**, *129*, 9044 – 9048.
[22] D. E. Discher, A. Eisenberg, *Science* **2002**, *297*, 967 – 973.

